Liquid−Solid Transition of Confined Water in Silica-Based Mesopores

Xiao X. Liu,[†,‡] Qiang Wang,[*,†] Xiu F. Huang,[†] Su H. Yang,[†] Chen X. Li,[†] Xiao J. Niu,[†] Qin F. Shi,[‡] Gang Sun,[†] and Kun Q. Lu[†]

Beijing National Laboratory for Condensed Matter Physics and Key Laboratory of Soft Matter Physics, Institute of Physics, Chinese Academy of Sciences, Beijing 100190, China and Department of Physics, Beijing Institute of Technology, Beijing 100081, China

Received: September 21, 2009; Revised Manuscript Received: February 21, 2010

Cooling and heating curves of water confined in partially filled Vycor porous glass were measured for both adsorption and desorption processes. One endothermic and two exothermic peaks were observed for almost all cases. The peak temperature and the enthalpy of the exothermic peak located below 232 K increased initially and then decreased with further increases in the filling factor. These abnormal changes were analyzed based on the liquid−solid transition of nanoconfined water using a core/shell model, and the initial adsorption process of water in this typical mesoporous material with disordered pores is discussed. In addition, an interesting observation is that different peak temperatures for the endothermic peak and an almost constant peak temperature for the exothermic peak were observed at the same filling factor obtained under different sample preparation conditions, that is, adsorption and desorption processes. To compare with the liquid−solid transition temperatures of confined water in fully filled silica-based mesopores of different pore radius, a parameter of the ratio of pore inner surface area to confined liquid volume is proposed in this paper. Referring to this parameter, the core part of confined water in silica-based nanopores has the same liquid−solid transition temperatures. This suggestion is valid for the freezing process of water confined in either fully filled ordered or fully or partially filled disordered pores. For the melting process, different linear changes of melting temperature with the ratio of pore inner surface area to liquid volume were observed for water in disordered and ordered pores.

1. Introduction

The liquid−solid transitions of water confined in silica-based mesopores have been extensively investigated for both fundamental and practical interests.[1−6] A depression of the transition temperature was observed when decreasing the hydrophilic pore radius R, and the dependence of the melting (or freezing) point depression $\Delta T_m = T_m(\text{bulk}) - T_m(\text{pore})$ (or $\Delta T_f = T_f(\text{bulk}) - T_f(\text{pore})$) on R has been linearly fitted using the modified Gibbs−Thomson equation:[4,7−10] $\Delta T_m = T_m(\text{bulk}) - T_m(\text{pore}) = (\alpha)/(R - \tau)(V_s T_m \gamma_{sl})/(\Delta H_m)$, where τ is the thickness of the nonfreezing water strongly bound to the surface of pore wall, V_s is the molar volume of solid, T_m is the melting temperature of bulk water, γ_{sl} is the surface tension between liquid and solid water, ΔH_m is the melting enthalpy of bulk water, and α is a constant. This classical approach has been found to be valid for water and some organic liquids[11] confined in porous silica with either ordered or disordered pores.[4,5,8−11] Ordered porous silica includes MCM-41 and SBA-15, among others,[4,8,9] whereas disordered porous silica includes controlled pore glass, some kinds of sol−gel silica, and the Vycor porous glass used in this paper.[5,10,11] In the Gibbs−Thomson equation, α depends on the topological structure of pores, for example, $\alpha = 3$ for spherical pores and 2 for cylindrical pores,[12] and is different depending on whether one is describing ΔT_m or ΔT_f.[8,12,13] To apply the Gibbs−Thomson equation to a more general case, $\alpha/(R - \tau)$ was replaced by S_p/V_p and $\partial S_p/\partial V_p$ to describe ΔT_f and ΔT_m, respectively.[14] Here, S_p is the inner surface area of pore and V_p is the pore volume.

The inadequacy of the Gibbs−Thomson equation for nanoconfined water was also pointed out by other authors, who found a deviation of the melting point from linearity when the pore radius is less than ∼1.5 nm.[15,16] These authors suggested that the temperature variations of γ_{sl}, ΔH_m, and V_s should be taken into account.[15] Actually, the temperature effect on $\gamma_{sl}/\Delta H_m$ had already been discussed by Turnbull, who found that $\gamma_{sl}/\Delta H_m = \lambda/a_m$, where λ is a constant and a_m represents the area per surface atom.[17] In other words, the temperature dependencies of γ_{sl}, ΔH_m,and V_s are largely compensated by each other in the Gibbs−Thomson equation.[18] This behavior may be one of the reasons why the parameters taken from normal conditions can be successfully used even in the supercooled state.

Another major concern regarding the liquid−solid transition of water confined in porous silica is the thickness τ of the nonfreezing water layer strongly bound to pore wall. Based on studies using differential scanning calorimetry (DSC) and nuclear magnetic resonance (NMR), Rennie and Clifford found no sign of freezing or melting when the thickness of the water film on the pore surfaces was less than about three monolayers.[19] Subsequently, different values of τ, from 0.38 to 1.2 nm, were reported, with the value depending on the topological structure and radius of the pores.[6,20−25] Generally speaking, γ_{sl} in the Gibbs−Thomson equation should be replaced by $\gamma_{sw} - \gamma_{lw}$ ($= \gamma_{sl}\cos\theta$). Here, γ_{sw} (γ_{lw}) represents the surface tension between the pore surface and the confined solid (confined liquid). The contact angle θ is formed by the ice/water interface with the wall. Because this thin nonfreezing water layer is

* To whom correspondence should be addressed. E-mail: qwang@aphy.iphy.ac.cn. Phone: 86-10-82649090. Fax: 86-10-82640224.
† Chinese Academy of Sciences.
‡ Beijing Institute of Technology.

10.1021/jp909108u
Published on Web 03/05/2010

adsorbed on the pore surfaces, the water/porous silica system can be regarded as a complete wetting case, and $\gamma_{sw} - \gamma_{lw} = \gamma_{sl}$.

At the same time, the structure of the solidified-phase of confined water has also been widely studied. During the past several decades, NMR, X-ray diffraction, and neutron scattering techniques have been used to reveal the structure of the low-temperature phase of water within ordered[5,26−28] and disordered silica pores.[15,28−34] A defective form of cubic ice (ice I_c), as opposed to the stable hexagonal phase (ice I_h), was mainly observed when cooling water in silica pores with $R < 15$ nm. More recently, neutron diffraction measurements indicate that the solidification of pore water creates a mixture that incorporates hybrid crystallites of ice I_h, ice I_c, and an amorphous form of ice with an intermediate density.[35,36] This fact suggests that the liquid−solid transition of water in silica pores is far more complex than previously thought.

All the results mentioned above were mainly extracted from fully filled silica pores with various R. Relatively speaking, too few experiments have been performed to evaluate the effect of the filling fraction ϕ on the liquid−solid transition of confined water. Within the limited publications, some inconsistent results have been reported even for the same confinement system.[6,33,37] These inconsistencies may result from the different pore shapes, detection methods, and experimental conditions, for example, cooling/heating rate, sample content, etc. A partially consistent observation is that there are two or three exothermic peaks on the DSC cooling curves of water in partially filled pores.[6,20,33] Some exothermic peaks depend on the pore radius and ϕ,[6] whereas an exothermic peak around 235 K is less dependent on ϕ.[33] This observation supports the coexistence of two or three types of water in the pores. For example, one type of water presents in the central region of the pores (defined herein as core water), and some water molecules locate between core water and bound water (defined herein as shell water). The nature of low-temperature phase transition (around 235 K) was attributed to the freezing[4,33,35] or glass transition[38] of shell water and the liquid−liquid transition of bound water,[39,40] respectively.

One issue is that the ϕ interval used by all publications was too large, leading to a lack of detailed understanding about the effect of ϕ on T_m or T_f, especially under low ϕ conditions. The studies performed under low ϕ conditions can adequately provide information on the effect of interfacial action between the pore surface and water on the liquid−solid transition of the water film on the pore surface. This is because increasing numbers of water molecules are located close to the pore wall with decreasing ϕ. Therefore, it is very important to study the liquid−solid transition of water within partially filled pores in detail. In addition, adsorption hysteresis is a typical characteristic of mesopores so it is also interesting to track the liquid−solid transition of confined water during adsorption and desorption processes. To meet these needs, ϕ was changed in small-intervals in this work and its effect on the liquid−solid transition of water in Vycor was studied in detail using DSC. The results are compared widely with those obtained from fully filled mesoporous silica with different R.

2. Experimental Details

Vycor glass (Corning, code 7930; average pore diameter, 7.6 nm; inner surface area, 122.5 m^2/g) was used as the porous matrix. As described in detail by Christenson[2] and Levitz,[41] and as seen from the Web site of the Corning Company, Vycor porous glass is formed by quenching and subsequent acid leaching of a SiO_2, B_2O_3, Na_2O, Al_2O_3+ZrO_2 melt, wherein the final concentrations of the four components are about 96%, 3%, 0.04%, and <1%, respectively. Therefore, Vycor glass can be considered simply as a silica-based mesoporous material, which consists of a network of essentially cylindrical pores with varying degrees of connectivity.[2]

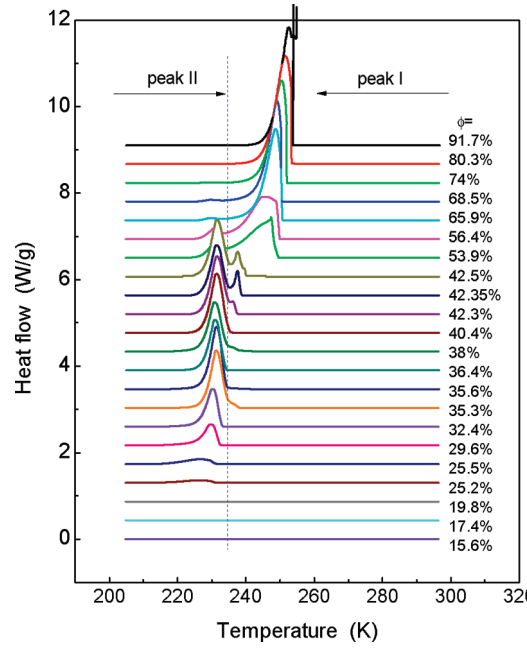

Figure 1. Cooling curves for water at several filling fractions. The curves are shifted upward in steps of 0.43 W/g. Measurements were made at a scanning rate of 5 K min^{-1}.

Before adsorption and desorption processes, Vycor was washed in 30% hydrogen peroxide at 90 °C for 4 h and then heated in distilled water at 90 °C for 4 h. This wash process was repeated several times until the C−H vibrational mode disappeared in the Raman spectrum of the sample being treated.[42] The clean Vycor was then slowly heated to 90 °C under vacuum to obtain dry Vycor. Ten samples of dry Vycor (about 1.2 g) were placed in the adsorption/desorption cell to precisely determine ϕ. The relative humidity was adjusted by changing the mixture ratio of saturated water vapors and pure nitrogen gas.[43] At some relative humidity points, two days were required to ensure adsorption/desorption equilibrium.[42] The sample weights were measured on a Mettler AE240 analytical balance with a sensitivity of 0.01 mg. After obtaining the absolute water content, ϕ was calculated by dividing by the water content in fully filled Vycor. During DSC measurements, at each ϕ level, a single piece of Vycor disk was hermetically sealed in an Aluminum standard crucible. After DSC measurement, the Vycor sample was taken out of the crucible and weighted. Less than a 1% change in water content was observed.

TA Instruments Q2000 differential scanning calorimeter was used at a scanning rate is of 5 K min^{-1}. The instrument was calibrated by bulk water and high purity indium (99.999 wt %) for determining T_m and calculating ΔH_m. Using three independent measurements, the errors in transition temperature and enthalpy change were about ±1.4 and ±3.2%, respectively.

3. Results

Experiments were performed for both adsorption and desorption processes. For brevity, only the cooling and heating curves for the adsorption process are shown in Figures 1 and 2 at several ϕ levels. All DSC curves were normalized by their respective water contents. For convenience, the subscripts "f-ad" (or "m-ad") and "f-de" (or "m-de") are used to denote the

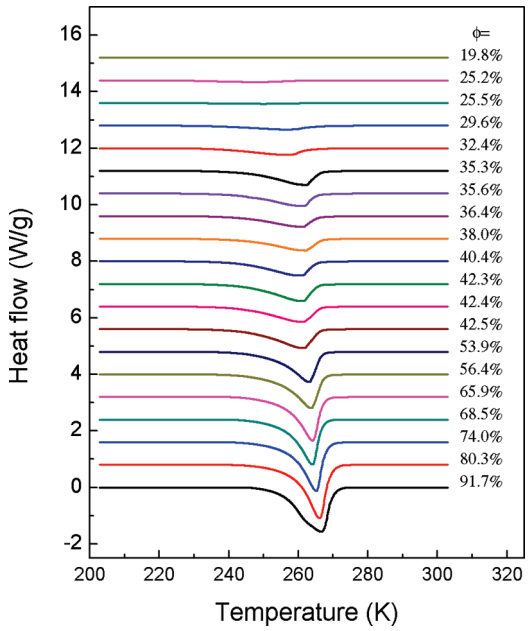

Figure 2. Heating curves for water at several filling fractions. The curves are shifted upward in steps of 0.8 W/g. Measurements were made at a scanning rate of 5 K min^{-1}.

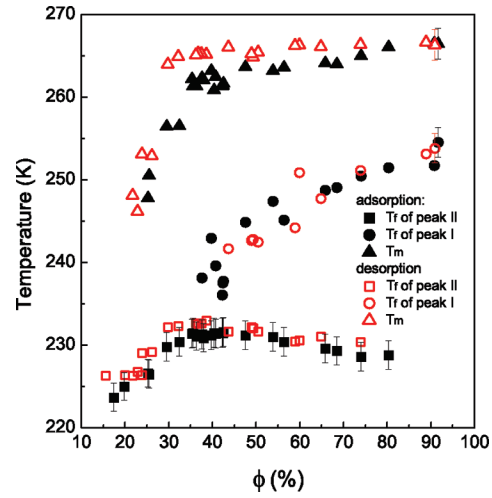

Figure 3. Freezing and melting temperatures as functions of filling fraction for the adsorption (solid symbols) and desorption (open symbols) processes, respectively. Temperature is taken from the peak temperature of the scanning curves.

freezing (or melting) process of confined water under adsorption and desorption processes, respectively.

3.1. The Cooling Process. As shown in Figure 1, no exothermic peak can be observed below $\phi = 15.6\%$. This is consistent with the result obtained previously that there is nonfreezing water bound on the hydrophilic silica-pore surfaces. Considering that the thickness of bound water is sensitive to the confinement condition, we first discuss the thickness of the nonfreezing bound water in Vycor. From the density of bulk water, the effective diameter of a water molecule is deduced to be 0.386 nm.[15,44] For the Vycor used in this paper (inner surface area 122.5 m^2/g), a densely packed monomolecular water layer on the pore wall will consist of ~1.07 mM of water per gram of Vycor, that is, $\phi \approx 10\%$. It appears that the nonfreezing bound water film should be thicker than one monolayer. However, as observed by Raman measurements, the vibrational mode of free OH on the pore surface cannot be detected only below $\phi \approx 18\%$.[42] This value is higher than that needed to form a complete monolayer coverage of physisorbed water, that is, $\phi \approx 10\%$ and suggests that the pore surface of Vycor is still only partially covered with adsorbed water even at $\phi = 15.6\%$.

When increasing ϕ to 17.4%, a small, broad exothermic peak at ≈223 K begins to show on the cooling curve. This behavior differs from that observed in the water/Vycor ($R = 2$ nm) system by Tombari et al.[44] There, a small exothermic peak at ≈233 K that already existed on the cooling curve even when the adsorbed water content was not sufficient to form a monolayer on the pore wall.[44] Tombari et al. suggested that small water clusters have formed on the inner surface of Vycor ($R = 2$ nm) before complete coverage of the pore surfaces by adsorbed water molecules. The difference between this work and ref 44 may result from the different sample treatment temperatures. Treatment temperature affects the SiOH density on the pore surfaces of Vycor. Tombari et al. adopted a higher treatment temperature, 413 K, than the 363 K used in this work. Higher treatment temperatures can reduce the SiOH density and favor the formation of water clusters, due to a reduction in the number of adsorption sites on the pore walls of porous silica.[45]

The freezing temperature of 223 K obtained at $\phi = 17.4\%$ is similar to the T_f value of water physisorbed on the silica surface.[46−48] The cooling curves of water films on silica surfaces with different layer thicknesses were measured by Nakamura et al.[48] They observed that an exothermic peak at ≈225 K remained almost constant as long as the water film was no less than two layers thick. Decreasing the water film thickness to only about a monolayer eliminated the exothermic peak. We want to stress that the exothermic peak at ≈223 K, observed in this work, is very similar to that observed by Nakamura et al. for the bilayer condition. The presence of the vibrational mode of free OH on the pore surface of Vycor, even at $\phi \approx 18\%$, does not support the typical layer-by-layer adsorption model, observed in the water/SBA-15 system.[49] The initial exothermic peak observed is similar to that of bilayer adsorbed water film, which suggests that a coupled growth model of a bilayer water film can be regarded as the main initial adsorption process for water in Vycor ($R = 3.8$ nm, treated at 363 K). According to this adsorption model, a bilayer water film will be formed once the pore surface is completely covered with adsorbed water. Consequently, this paper suggests that the thickness of nonfreezing bound water in Vycor ($R = 3.8$ nm, treated at 363 K) is a single monolayer and the exothermic peak observed at $\phi = 17.4\%$ is attributed to the liquid−solid transition of the first layer of the shell water.

As shown in Figure 1, when increasing ϕ from 17.4 to ≈40%, the exothermic peak becomes increasingly obvious, accompanied by an increase in T_f from ≈223 to ≈232 K. T_f and the integral quantity of the exothermic peak, ΔH_f, are plotted in Figures 3 and 4, respectively, as a function of ϕ. As seen in these two figures, T_f and ΔH_f increase with increasing ϕ within $17.4\% < \phi < \approx 40\%$. Two factors can result in these increases. One factor is that the thickness of the water film taking part in the liquid−solid transition increases with increasing ϕ, referring to a radial-growth model of the adsorbed water within $17.4\% < \phi < \approx 40\%$. The other factor is the radius of the neck pore fully filled by water taking part in the liquid−solid transition increases with increasing ϕ, referring to an axial-growth model of the adsorbed water within the same ϕ range. As mentioned in the experimental section, the neck pore of Vycor can be regarded as a cylindrical pore, so the Gibbs−Thomson equation is still valid. According to $\Delta T = 2\gamma_{ls}V_mT_0/(\Delta H_f(R - \tau))$, where γ_{ls}= 30 ergs/cm^2, $\Delta H_f = 6.01$ kJ/mol, $V_m = 18$ cm^3/mol, and $\tau = 0.386$ nm, it can be calculated that $R = 2.0$ nm when $T_f = 232$ K. As illustrated in Figures 1 and 3, the exothermic peak at

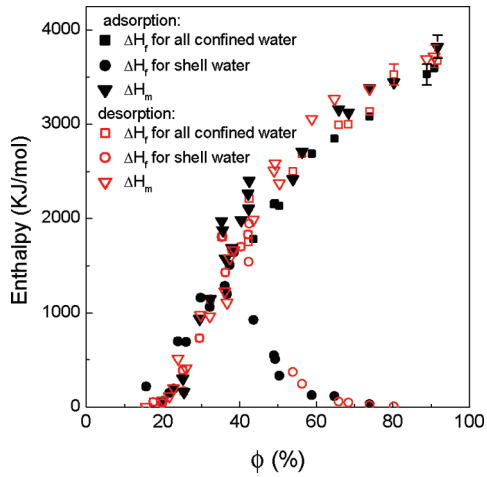

Figure 4. Freezing and melting enthalpies of water within Vycor at different filling fractions for adsorption (solid symbols) and desorption (open symbols) processes, respectively.

232 K corresponds to the liquid−solid transition of confined water at $\phi \approx 40\%$. If the exothermic peak below 232 K mainly reflects the liquid−solid transition of water within fully filled neck pores, then the pores with $R \leq 2.0$ nm will occupy ≈40% of the free volume of Vycor. However, as obtained from BJH adsorption reports, the neck pores with $R \leq 2.0$ nm only occupy ≈5% of the free volume of Vycor. This large difference between theory and experimental measurement indicates that the exothermic peaks below 232 K (defined as peak II in this paper) mainly correspond to the liquid−solid transition of water films on the pore surface of Vycor. In other words, the first possibility mentioned above is dominant for the water/Vycor system below $\phi \approx 40\%$.

Above $\phi = 40\%$, another exothermic peak, above 232 K (defined as peak I), begins to appear and becomes increasingly obvious with increasing ϕ. On the contrary, peak II becomes progressively weaker and almost vanishes at $\phi \approx 80\%$. As shown in the adsorption−desorption isotherm of water/Vycor (Figure 3 of ref 42), capillary condensation occurs at $\phi \approx 40\%$. Therefore, core water begins to form above $\phi = 40\%$. It is reasonable to attribute peak I to the liquid−solid transition of core water.

Figures 1, 3, and 4 illustrate the decrease in T_f and ΔH_f of shell water when increasing the core water content within the range $40 < \phi < 80\%$. Similar behavior was also found in Ar/Vycor and Ar/SBA-15 systems.[50,51] It was suggested that core liquid in the filled part of the pores freezes at higher temperature; shell liquid in pore segments without core liquid, however, remains in the liquid state down to lower temperatures, at which it delayers and joins the solidification of core liquid.[4,50,51] According to this model, the solid phase previously formed at higher temperature can act as a growth substrate of shell liquid at lower temperature. On the basis of the lattice matching principle, only one solidification structure should be detected. However, a mixed-phase was found in water/SBA-15, which incorporates hybrid crystallites of ice I_h and ice I_c in an amorphous ice.[35,36]

On the basis of the contradiction mentioned above and the effect of ϕ on the T_f and ΔH_f of peak II within $15.6 < \phi < 80\%$, this paper suggests that the liquid−solid transition of shell water may take place independently in pore segments without core water. Within $40 < \phi < 80\%$, partially filled pores of Vycor can be regarded simply as being covered with shell water films along the pore radius and filled by discontinuous core water segments along the axial direction. The fraction of core water decreases in the axial direction with decreasing ϕ within $40 < \phi < 80\%$. At a corresponding temperature, the liquid−solid transition of core water takes place first. At the same temperature, part of the shell water delayers and joins the freezing process of the core water.[50,51] More core water will result in more shell water molecules joining the freezing of core water. Subsequently, partial shell water still exists in the liquid state and its thickness decreases with an increasing fraction of core water within $40 < \phi < 80\%$. With further decrease in temperature, the liquid−solid transition of shell water may take place independently in pore segments without core water. The dependencies of T_f and ΔH_f on the thickness of the water film observed within $\phi < 40\%$ should still be effective. Therefore, this reasonably explains the increase in T_f and ΔH_f for shell water with decreasing ϕ within $40 < \phi < 80\%$. In addition, low-temperature Raman measurements, being carried out in our research group may be helpful in revealing the structures of the solidified phase for shell water films of different thickness. A hypothesis can be proposed that the solidified-phase of shell water should have a more disordered structure with decreasing thickness.

3.2. The Melting Process of Confined Water. For the melting process, only one, unsymmetrical, broad endothermic peak was observed for all filling fractions. Kuchta analyzed the influence of the pore wall roughness on the melting mechanism of monolayers adsorbed in cylindrical pores.[52] It was suggested that, for heterogeneous pores, some adsorbed molecules are still trapped in strongly attractive adsorption sites even when the melting starts at a relatively low temperature. This analysis can explain the broad endothermic peak observed in this work at lower ϕ.

An interesting behavior, shown in Figure 3, is that $T_{m-de} > T_{m-ad}$, especially within the adsorption hysteresis region, that is, $30 < \phi < 80\%$. Adsorption hysteresis is a typical characteristic of mesoporous materials. Recently, using NMR techniques and Vycor porous glass as a model mesoporous system, Valiullin found that, within the adsorption hysteresis region, the dynamics of liquid confined in silica porous glass is mainly dominated by a slow density rearrangement.[53] In other words, it is not driven by a global equilibration—the distribution of the initially formed liquid "droplets" only represents some local minima of the free energy. The arrangement of these liquid droplets is a much slower process. This nonequilibrium process will result in a different distribution of confined water for the same adsorbed amount when obtained from adsorption or desorption. As confirmed in our previous paper, at some adsorbed amounts within the adsorption hysteresis region, the density of confined water prepared upon desorption is lower than that obtained upon the adsorption process.[42] In general, low-density water has a low T_f or T_m, which is applicable to interfacial water and water within a small confinement size. Consequently, it can be deduced that $T_{m-de} < T_{m-ad}$ or $T_{f-de} < T_{f-ad}$ within the adsorption hysteresis region. This deduction is partially supported by the results obtained from the cooling process, where T_{f-ad} is slightly higher than T_{f-de} within $40 < \phi < 60\%$. On the contrary, as pointed out at the beginning of this paragraph, $T_{m-de} > T_{m-ad}$, especially within $30 < \phi < 80\%$. This deviation between the deductions mentioned above and the experimental results confirms a redistribution of water molecules in pores of Vycor during the collective freezing process.

4. Discussion

As briefly reviewed in the introduction section, for water within fully filled silica-based mesoporous materials, the

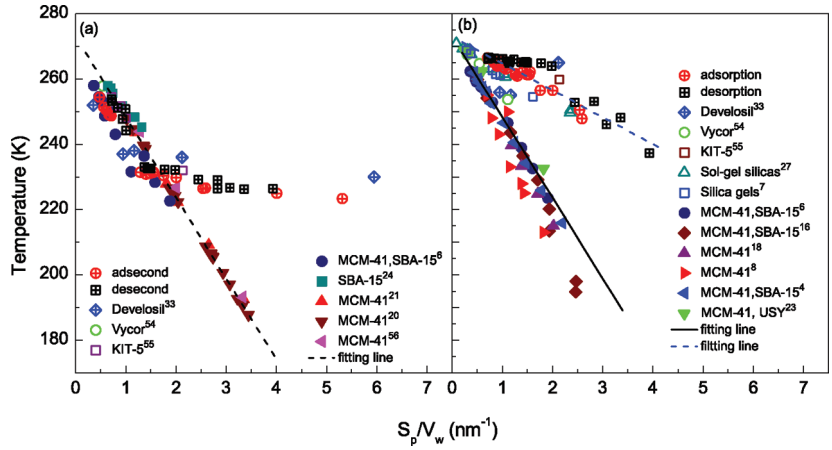

Figure 5. (a) Freezing temperature as a function of the ratio of inner surface area of pores to the water volume for water within silica-based mesoporous materials with fully filled ordered pores (solid symbols), partially (cross-filled symbols) and fully (open symbols) filled disordered pores. Fitting line: $T_f = T_f^0 - (\nu\gamma_{sl}T_f^0/\Delta H_f)(S_p/V_w)$. (b) Melting temperatures of water within ordered fully filled pores (solid symbols), partially (cross-filled symbols) and fully (open symbols) filled disordered pores. Solid line: $T_m = T_m^0 - (\nu\gamma_{sl}T_m^0/\Delta H_m)(S_p/V_w)$, dashed line: $T_m = T_m^0 - [\nu\gamma_{sl}T_m^0/(6\Delta H_m)](S_p/V_w)$. It should be stressed that the increase in S_p/V_w corresponds to two different processes for fully filled and partially filled pores. For fully filled pores, increasing S_p/V_w corresponds to decreasing the radius of pores. For partially filled pores, increasing S_p/V_w corresponds to decreasing filling fraction.

Gibbs−Thomson equation can be perfectly applied to describe the linear relation between ΔT_m or ΔT_f and $1/(R - \tau)$. However, for the liquid−solid transition of water within partially filled mesopores, because few measurements have been reported, it is still unclear how to describe the change of ΔT_m or ΔT_f with hydration levels. This section discusses this question. Some conclusions, together with some remaining questions, are identified.

Referring to S_p/V_p, a parameter S_p/V_w was proposed in this paper to describe ΔT_m or ΔT_f obtained under different ϕ. Here, V_w is the volume of confined water and can be regarded as the water content if the change in density of water with R and ϕ is neglected. For fully filled pores, $S_p/V_w = S_p/V_p$. It should be stressed that the nonfreezing bound water should be subtracted before the calculations of S_p and V_w.

In this paper, S_p/V_w was calculated based on the following methods. (1) For fully filled ordered pores, for example, SBA-15 and MCM-41, $S_p/V_w = 2/(R - \tau)$. (2) For porous materials with either ordered or disordered pores, S_p/V_w was calculated directly only if S_p, V_p, R and τ were reported. (3) For partially filled Vycor, $S_p/V_w = 109.6/[(\phi - 0.1) \times 0.246]/1000$ nm^{-1}. Here, 109.6 m^2/g is the inner surface area of Vycor after subtracting the section of nonfreezing bound water. In addition, for the water/Vycor system, T_f is extracted from peak I (or peak II) when $\phi > 40\%$ (or $\phi < 40\%$).

Figure 5a shows T_f as a function of S_p/V_w for water within fully and partially filled ordered and disordered silica-based mesopores. It can be seen that confined water has almost constant T_f only under a constant S_p/V_w condition when $S_p/V_w < 1.4$ nm^{-1}, where the relationship between T_f and S_p/V_w can be linearly fitted by $T_f = T_f^0 - (\nu\gamma_{sl}T_f^0/\Delta H_f)(S_p/V_w)$. Here, T_f^0 is the freezing temperature of bulk water. Compared with the normal Gibbs−Thomson equation, the only change in this linear function is to replace S_p/V_p by S_p/V_w. In general, the Gibbs−Thomson equation can be viewed as a description of the curvature-dependent depression of freezing or melting point. Apparently, the Gibbs−Thomson equation cannot be used to evaluate T_f of water within partially filled pores, which has only a constant radius of curvature. However, Figure 5a illustrates that the Gibbs−Thomson equation can be adopted to perfectly describe the change in T_f obtained from partially filled states.

When $S_p/V_w > 1.4$ nm^{-1}, T_f still decreases linearly with increasing S_p/V_w for water within fully filled pores, whereas it is almost insensitive to S_p/V_w for water within partially filled Vycor. This obvious difference suggests that it is the radius of curvature of the pore not the interfacial effect that mainly determines T_f of water when $S_p/V_w > 1.4$ nm^{-1} (For fully filled porous silica with ordered pores, $R \leq 1.7$ nm as $S_p/V_w \geq 1.4$ nm^{-1}. For partially filled Vycor, $\phi \leq 40\%$ as $S_p/V_w \geq 1.4$ nm^{-1}). This suggestion is reasonable if the fact is considered that the liquid−solid transition is a collective process and does not begin until the size of embryos exceeds a critical value. Figure 5a indicates that this transition process can be hindered more effectively by the size scale than the interfacial effect.

The dependence of T_m on S_p/V_w is summarized in Figure 5b (There, solid symbols refer to T_m of water in fully filled ordered pores; Cross-filled and open symbols refer to T_m of water in partially and in fully filled disordered pores, respectively.). As compared with T_f vs S_p/V_w, the change of T_m with S_p/V_w depends strongly on pore shape. For water within idealized cylindrical pores (solid symbols), $T_m = T_m^0 - (\nu\gamma_{sl}T_m^0/\Delta H_m)(S_p/V_w)$, where T_m^0 is the melting point of bulk water. For water confined in disordered silica pores (cross-filled and open symbols), such as KIT-5, Vycor, controlled porous glass, and Develosil, $T_m = T_m^0 - [\nu\gamma_{sl}T_m^0/(6\Delta H_m)](S_p/V_w)$. Figure 5b confirms the results reported by Brun that T_m depends more sensitively on the geometrical structure of pores compared with T_f.[13] In addition, a new result, shown in Figure 5b, is that water molecules in either partially or fully filled disordered pores have a very similar T_m only under the same S_p/V_w condition.

In addition to the results described above, some remaining questions also should be pointed out at the end of this paper. As illustrated herein, there are three kinds of water within Vycor glass: nonfreezing bound water; core water formed during the capillary condensation process; and shell water located between bound and shell water. Core-water and partial shell water freeze at different temperatures, as shown in Figure 3. However, the volumes of shell and core water are both included during the calculation of S_p/V_w. For core water, the relationship between T_f and S_p/V_w does not depend on V_w only taken from core water. This misgiving can be dispelled when $\phi > 60\%$, where almost all shell water joins the liquid−solid transition of core water at

high temperature. The residual question is why the change of T_f with S_p/V_w can be linearly fitted well within $40 < \phi < 60\%$, that is, $0.9 < S_p/V_w < 1.4$ nm^{-1}.

5. Conclusion

In summary, first, this paper suggests that a bilayer water film will be formed once the pore wall is completely covered with adsorbed water. Second, it is stressed that the amount of shell water joining the solidification of core water increases with an increase of core water content above $T = 232$ K. With further decrease in temperature, the liquid−solid transition of the residual shell water takes place at the pore segments where there is no core water. The latter process may be independent of the solidified phase of core water. Third, for the same filling fraction, water molecules have a very similar freezing temperature but a different melting temperature when the sample is prepared by adsorption and desorption processes, respectively. Finally, the puzzling behavior has been observed for the first time, that water molecules in different types of pores have almost the same freezing temperature under the same S_p/V_w condition when $S_p/V_w < 1.4$ nm^{-1}. This case is valid for both fully filled ordered and fully or partially filled disordered silica-based mesopores. For the melting process, two kinds of linear dependence of melting temperature on S_p/V_w were confirmed for water confined in ordered and disordered pores, respectively. In addition, for disordered pores, a similar melting temperature was observed under the same S_p/V_w, independent of the filling state of pores.

Acknowledgment. We thank the referees for their comments and suggestions. X. X. L. thanks Dr. Jun Li of Tsinghua University for his experimental support. This work was supported by NSFC (Grant Nos. 10574145, 10874208, and 10675018), the National Basic Research Program of China (Grant No. 2004CB619005), and the Key Item of Knowledge Innovation Project of Chinese Academy of Sciences (Grant No. KJCX2-YW-M07).

References and Notes

(1) Gelb, L. D.; Gubbins, K. E.; Radhakrishnan, R.; Bartkowiak, M. S. *Rep. Prog. Phys.* **1999**, *62*, 1573.
(2) Christenson, H. K. *J. Phys.: Condens. Matter* **2001**, *13*, R95.
(3) Alba-Simionesco, C.; Coasne, B.; Dosseh, G.; Dudziak, G.; Gubbins, K. E.; Radhakrishnan, R.; Sliwinska-Bartkowiak, M. *J. Phys.: Condens. Matter* **2006**, *18*, R15.
(4) Findenegg, G. H.; Jahnert, S.; Akcakayiran, D.; Schreiber, A. *ChemPhysChem* **2008**, *9*, 2651.
(5) Webber, J. B. W.; Dore, J. C.; Strange, J. H.; Anderson, R.; Tohidi, B/initials> *J. Phys.: Condens. Matter* **2007**, *19*, 415117.
(6) Schreiber, A.; Ketelsen, I.; Findenegg, G. H. *Phys. Chem. Chem. Phys.* **2001**, *3*, 1185.
(7) Ishikiriyama, K.; Todoki, M. *Thermochim. Acta* **1995**, *256*, 213.
(8) Morishige, K.; Kawano, K. *J. Chem. Phys.* **1999**, *110*, 4867.
(9) Webber, J. B. W.; Strange, J. H.; Dore, J. C. *Magn. Reson. Imag.* **2001**, *19*, 395.
(10) Landry, M. R. *Thermochim. Acta* **2005**, *433*, 27.
(11) Jackson, C. L.; Mckenna, G. B. *J. Chem. Phys.* **1990**, *93*, 9002.
(12) Faivre, C.; Bellet, D.; Dolino, G. *Eur. Phys. J. B* **1999**, *7*, 19.
(13) Brun, M.; Lallemand, A.; Quinson, J.-F.; Eyraud, C. *Thermochim. Acta* **1977**, *21*, 59.
(14) Petrov, O.; Furó, I. *Phys. Rev. E* **2006**, *73*, 011608.
(15) Tombari, E.; Salvetti, G.; Ferrari, C. *J. Chem. Phys.* **2005**, *122*, 104712.
(16) Kittaka, S.; Ishimaru, S.; Kuranishi, M.; Matsuda, T.; Yamaguchi, T. *Phys. Chem. Chem. Phys.* **2006**, *8*, 3223.
(17) Turnbull, D. *J. Appl. Phys.* **1950**, *21*, 1022.
(18) Jahnert, S.; Chavez, F. V.; Schaumann, G. E.; Schreiber, A.; Schonhoff, M.; Findenegg, G. H. *Phys. Chem. Chem. Phys.* **2008**, *10*, 6039.
(19) Rennie, G. K.; Clifford, J. *J. Chem. Soc., Faraday Trans. 1* **1977**, *73*, 680.
(20) Hansen, E. W.; Stöcker, M.; Schmidt, R. *J. Phys. Chem.* **1996**, *100*, 2195.
(21) Schmidt, R.; Hansen, E. W.; Stöcker, M.; Akporiaye, D.; Ellestad, O. H. *J. Am. Chem. Soc.* **1995**, *117*, 4049.
(22) Rault, J.; Neffati, R.; Judeinstein, P. *Eur. Phys. J. B* **2003**, *36*, 627.
(23) Janssen, A. H.; Talsma, H.; van Steenbergen, M. J.; de Jong, K. P. *Langmuir* **2004**, *20*, 41.
(24) Endo, A.; Yamamoto, T.; Inagi, Y.; Iwakable, K.; Ohmori, T. *J. Phys. Chem. C* **2008**, *112*, 9034.
(25) Smirnov, P.; Yamaguchi, T.; Kittaka, S.; Takahara, S.; Kuroda, Y. *J. Phys. Chem. B* **2000**, *104*, 5498.
(26) Morishige, K.; Nobuoka, K. *J. Chem. Phys.* **1997**, *107*, 6965.
(27) Webber, B.; Dore, J. *J. Phys.: Condens. Matter* **2004**, *16*, S5449.
(28) Morishige, K.; Yasunaga, H.; Uematsu, H. *J. Phys. Chem. C* **2009**, *113*, 3056.
(29) Li, J.-C.; Ross, D. K.; Benham, M. J. *J. Appl. Crystallogr.* **1991**, *24*, 794.
(30) Bellissent-Funel, M.-C.; Lai, J.; Bosio, L. *J. Chem. Phys.* **1993**, *85*, 4246.
(31) Baker, J. M.; Dore, J. C.; Behrens, P. *J. Phys. Chem. B* **1997**, *101*, 6226.
(32) Bruni, F.; Antonietta Ricci, M.; Soper, A. K. *J. Chem. Phys.* **1998**, *109*, 1478.
(33) Takamuku, T.; Yamagami, M.; Wakita, H.; Masuda, Y.; Yamaguchi, T. *J. Phys. Chem. B* **1997**, *101*, 5730.
(34) Fouzri, A.; Dorbez-Sridi, R.; Oumezzine, M. *J. Chem. Phys.* **2002**, *116*, 791.
(35) Seyed-Yazdi, J.; Farman, H.; Dore, J. C.; Webber, J. B. W.; Findenegg, G. H.; Hansen, T. *J. Phys.: Condens. Matter* **2008**, *20*, 205107.
(36) Seyed-Yazdi, J.; Farman, H.; Dore, J. C.; Webber, J. B. W.; Findenegg, G. H. *J. Phys.: Condens. Matter* **2008**, *20*, 205108.
(37) Morishige, K.; Iwasaki, H. *Langmuir* **2003**, *19*, 2808.
(38) Gallo, P.; Rovere, M.; Spohr, E. *J. Chem. Phys.* **2000**, *113*, 11324.
(39) Zanotti, J. M.; Bellissent-Funel, M. C.; Chen, S. H. *Europhys. Lett.* **2005**, *71*, 91.
(40) Zanotti, J. M.; Bellissent-Funel, M. C.; Kolesnikov, A. I. *Eur. Phys. J. Special Topic* **2007**, *141*, 227.
(41) Levitz, p.; Ehret, G.; Sinha, S. K.; Drake, J. M. *J. Chem. Phys.* **1991**, *95*, 6151.
(42) Huang, X. F.; Wang, Q.; Liu, X. X.; Yang, S. H.; Li, C. X.; Sun, G.; Pan, L. Q.; Lu, K. Q. *J. Phys. Chem. C* **2009**, *113*, 18768.
(43) Wang, L. W.; Wang, Q.; Li, C. X.; Niu, X. J.; Sun, G.; Lu, K. Q. *Phys. Rev. B* **2007**, *76*, 155437.
(44) Tombari, E.; Ferrari, C.; Salvetti, G.; Johari, G. P. *Thermochim. Acta* **2009**, *492*, 37.
(45) Bogdan, A.; Kulmala, M.; Avramenko, N. *Phys. Rev. Lett.* **1998**, *81*, 1042.
(46) Kinney, D. R.; Chuang, I.-S.; Maciel, G. E. *J. Am. Chem. Soc.* **1993**, *115*, 6786.
(47) Bogdan, A.; Kulmala, M.; Gorbunov, B.; Kruppa, A. *J. Colloid Interface Sci.* **1996**, *177*, 79.
(48) Nakamura, M.; Uematsu, H.; Seko, A.; Shiomi, H. *J. Cerm. Soc. Japan* **1997**, *105*, 1141.
(49) Grunberg, B.; Emmler, T.; Gedat, E.; Shenderovich, J.; Findenegg, G. H.; Limbach, H. H.; Buntkowsky, G. *Chem.—Eur. J.* **2004**, *10*, 5689.
(50) Wallacher, D.; Knorr, K. *Phys. Rev. B* **2001**, *63*, 104202.
(51) Ewing. G. E.; Foster. M.; Cantrell. W.; Sadtchenko. V. Thin film water on insulator surfaces. In *Water in Confining Geometries*; Buch, V., Devlin, J. P. Eds.; Springer-Verlag: Berlin, 2003; pp 179−211.
(52) Kuchta, B.; Firlej, L.; Denoyel, R.; Rols, S.; Johnson, M. R.; Coasne, B. *J. Chem. Phys.* **2008**, *128*, 184703.
(53) Valiullin, R.; Naumov, S.; Galvosas, P.; Karger, J.; Woo, H.-J.; Porcheron, F.; Monson, P. A. *Nature* **2006**, *443*, 965.
(54) Handa, Y. P.; Zakrzewski, M.; Fairbridge, C. *J. Phys. Chem.* **1992**, *96*, 8594.
(55) Morishige, K.; Yasunaga, H.; Denoyel, R.; Wernert, V. *J. Phys. Chem. C* **2007**, *111*, 9488.
(56) Akporiaye, D.; Hansen, E. W.; Schmidt, R.; Stocker, M. *J. Phys. Chem.* **1994**, *98*, 1926.

JP909108U